THE INTERNATIONAL JOURNAL OF MEDICAL ROBOTICS AND COMPUTER ASSISTED SURGERY
Int J Med Robotics Comput Assist Surg 2010; **6**: 102–112.
Published online 28 January 2010 in Wiley InterScience (www.interscience.wiley.com). **DOI:** 10.1002/rcs.297

ORIGINAL ARTICLE

The implementation of an integrated computer-assisted system for minimally invasive cardiac surgery

Junfeng Cai[1]
Zhe Luo[2]
Lixu Gu[3]*
Rong Xu[4]
Qiang Zhao[1]

[1]*Ruijing Hospital, Department of Cardiosurgery, 197 Rui Jin Er Road, Shanghai, People's Republic of China*

[2]*Shanghai JiaoTong University, School of Software, 800 Dongchuan Road, Min-Hang, Shanghai, People's Republic of China*

[3]*Shanghai JiaoTong University, Med-X Research Institute, 1954 Huashan Road, Shanghai, People's Republic of China*

[4]*Shanghai JiaoTong University, School of Mechanical Engineering, 800 Dongchuan Road, Min-Hang, Shanghai, People's Republic of China*

*Correspondence to: Lixu Gu, Shanghai JiaoTong University, Med-X Research Institute, 1954 Huashan Road, Shanghai, People's Republic of China.
E-mail: gulixu@sjtu.edu.cn

Accepted: 4 December 2009

Abstract

Background Preoperative planning and surgical navigation are two crucial aspects of a computer-assisted system for the success of minimally invasive cardiac surgery.

Methods In the first part, port placement planning was mainly discussed. We proposed an algorithm based on four criteria to achieve optimized placement. In the second part, an optical tracker was used to locate the thoracoscope and surgical instruments accurately and to show the relative positions between the thoracoscope, surgical instruments and the patient's anatomical structures. An image-matching technique was employed to help the surgeon locate the target, using real-time thoracoscopic video images during the procedure.

Results In order to verify our proposed algorithms, several clinical planning cases were performed to compare our port placement algorithm to the traditional method. Both phantom test and animal study experiments were also done to demonstrate the validity of the target tracking of the system. Both the phantom test and the animal study revealed that the fiducial registration error (FRE) was 1.08 ± 0.16 mm and system error was 5.05 ± 0.67 mm, respectively.

Conclusion A novel computer-assisted system for minimally invasive cardiac surgery has been developed. This method has shown its capability to achieve the preoperative planning and real-time surgery navigation. Copyright © 2010 John Wiley & Sons, Ltd.

Keywords minimally invasive cardiac surgery; image-guided surgery; port placement planning; image matching

Introduction

Minimally invasive cardiac procedures can potentially reduce the complications arising from surgical interventions by minimizing the size of the incision required to access the heart, while employing medical imaging to visualize intracardiac targets without direct vision (1). In recent years, there has been a progressive trend to use minimally invasive surgical techniques on cardiac surgery to reduce the side effects of surgical procedures (2).

Minimally invasive cardiac surgery is done using a thoracoscope and two surgical instruments that are inserted into the patient's chest through three ports that have been opened on the patient. However, the problem arises of locating the ports. Incorrect port placement will result in problems, e.g. the view of thoracoscope cannot cover the target, or the instruments cannot reach the surgical region, which not only affect the efficiency of the surgery but can also lead to failure of the surgery in the worst cases. Loulmet *et al*. (3) reported a clinical experiment of coronary artery bypass grafting (CABG) using the thoracoscope in 1999. Because of a lack of effective preoperative planning, they determined the port positions based on experience obtained from an experiment on eight corpses. In order to get the best three port positions, they made seven ports on each body, and tested them based only on surgical output. They finally proposed the rough anatomical positions of the ports, which have been widely accepted by most surgeons so far. However, large differences between patients' anatomical stuctures, dependence on experience and lack of a measurable standard are the disadvantages of this method. Chiu *et al*. (4) first proposed port placement planning research using a 3D image, where he used a three-dimensional (3D) model reconstructed from CT and MRI images of the patient's chest to rebuild the surgical environment model and simulate the surgery, according to the particular requirements of a coronary surgeon, to find the best approach. This original method has no specific measurement criteria, causing it to be limited to the satisfaction of the surgeon. Moreover this method did not take into account all the information obtained before surgery. However, it opened the way for using 3D images to do the preoperative planning of minimally invasive cardiac surgery. Sorensen *et al*. (5) researched port placement planning for cardiovascular surgery, focusing on simulation of the surgical environment and the process by which port placement planning could be obtained. Austad *et al*. (6) used the Zeus™ robot as a model to simulate the surgical environment in MATLAB, and researched port placement planning by measuring the angle and distance through the simulated motion range of surgical instruments. However, these researches into preoperative planning were still using two-dimensional (2D) images, which can not show the 3D anatomical structure. This is still a challenge for safe, surgeon-friendly and port placement-optimized preoperative planning. After that, Coste-Maniere *et al*. (7) and Adhmai and Coste-Maniere (8,9) researched the specific objective measure for the optimum of port placement planning on a 3D model constructed from CT images, focusing on the thoracoscope view and the motion range of the instruments. These traditional methods were not able to take 'comfort' into account. The 'comfort' factor can give the surgeon more freedom and room in manipulating the instruments, which can obviously reduce surgical time and improve surgical accuracy. We put the freedom of manipulating the instruments ('comfort') into the criterion and optimized the parameters reflecting more aspects related to port positions. Because the 'comfort' feeling is hard to quantify, we can only test it by a phantom study (as shown in Tables 2, 3). Clinical experience has shown that the 'comfort' factor can reduce surgical time and improve accuracy. The new proposed optimization criteria for port placement planning have been shown to be superior to the traditional ones in comfort, accuracy and efficiency by the surgeons who applied it to real surgical cases.

On the other hand, the entire traditional minimally invasive cardiac surgery procedure is guided solely by a 2D video thoracoscope, which only has a small field of view (10). It lacks real-time 3D guidance, which leads to the result that the surgeon can not locate the thoracoscope and surgical instruments accurately and establish the relative positions between the thoracoscope, the surgical instruments and the patient's anatomical structures. Intra-operative navigation systems that guide the surgeon to finish the surgery accurately after preoperative planning are also being researched and put into use by many research institutions, such as Swiss Federal Institute of Technology Zurich (ETH), National Institute for Research in Computer and Control Sciences (INRIA), and General Electric Company (GE) (11–13). Szpala *et al*. (2) have developed a virtual cardiac surgical platform that can integrate an endoscope with preoperative images to support the planning and guidance of cardiac intervention. The system proposed in this paper was inspired by their work on an optical tracker to locate the thoracoscope and surgical instruments accurately and to show the relative positions between them. The image-matching technique is employed to help the surgeon locate the target in real-time thoracoscopic video images during the procedure.

Under the consideration of smoothing the data flow between these two stages of minimally invasive cardiac surgery, this paper focuses on the implementation of an integrated system with both preoperative planning, using port placement planning improved from the traditional method, and intra-operative real-time navigation. The system was built under close cooperation with a cardiac surgeon working in a public hospital. The implementation of the whole system is introduced in this paper.

Materials and Methods

Architecture of the whole system

The proposed system was developed in a PC environment with Python and VTK development software. In order to make the data, control and display more independent, which improves the system's extensibility, we built the system using the MVC pattern (14). Figure 1 shows the whole architecture of the system.

Preoperative planning

After a patient's data had been processed by the image-processing module and the 3D modelling visualization module, 3D reconstruction models of the patient's heart and skeleton were constructed, on which the preoperative port placement planning was made. Here, we proposed a novel approach to conducting this process.

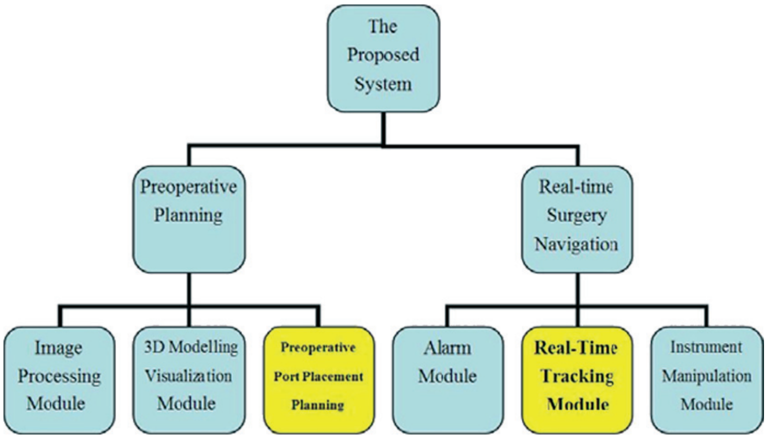

Figure 1. Hierarchy of the system's architecture

Parameter definition

First, we needed to define three parameters, α, β and d, as shown in Figure 2, where: α is the angle between the normal of the target and the direction of the line connecting the port and the target; β is the angle between the normal of the position of the port on the chest wall and the direction of the line connecting the port and the target centre; and d is the distance between the port and the target.

Optimization criteria

In order to ensure the reliability and validity of the result of the port placement planning, four criteria were employed according to relevant sources in the literature and the surgical experience of surgeons from the Zhongshan Hospital, Shanghai:

1. *The reachability criterion*. This criterion judges whether a surgical instrument is long enough to reach the target.
2. *The view of the thoracoscope (α angle) criterion*. The thoracoscope's lens is perpendicular to its axis. For the thoracoscope port, the smaller α is, the better view the surgeon can get. Therefore, α should be as small as possible and $<90°$ (9,15).
3. *The flexibility of the instrument (β angle) criterion*. The β angle actually shows the flexibility of the surgical instrument. The larger β is, the larger the motion range and the better the flexibility of the surgery instrument. However, when β is too large it will give the surrounding tissue extra pressure, which may cause unnecessary injuries (7,9,15,16). Thus, according to the surgeon's experience, the β angle should be as big as possible but $<60°$ (15) in atrial septal repair (ASR) and $<90°$ in CABG.
4. *The optimal triangle criterion ('comfort' factor)*. In minimally invasive cardiac surgery, one thoracoscope and two surgical instruments are used, hence there are three ports, forming a triangle. Taking the line segment between the two surgical instruments as the baseline, its length shows the possibility of collision between the two instruments (15,16). The quotient of the other two lines, i.e. length of the shorter one divided by the length of the longer one, expresses the symmetry of the triangle, which shows the 'comfort' of the operation. So both the quotient and the baseline are supposed to be as large as possible.

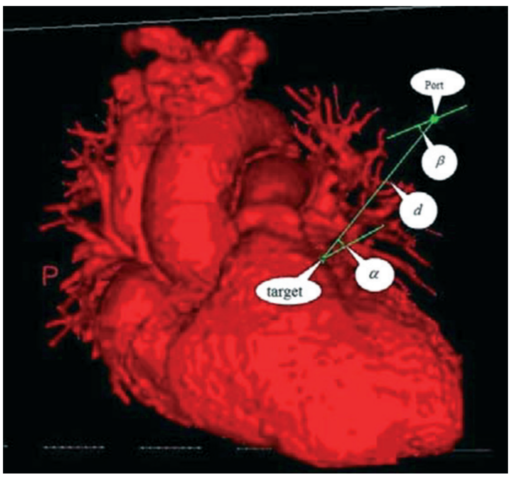

Figure 2. Parameter definition

The process of preoperative port placement planning

After a model of the heart and the skeleton have been constructed, the port placement planning can be started. First, we define the target and compute the normal of the target, then we compute the candidate positions and the directions from which the ports will be selected. Finally, the ports of the thoracoscope and the surgical instruments are selected according to the next procedure.

Calculation of the target

Surgeons can find the target on the model heart, but the surface of the target is not flat; thus, the normal of

DOI: 10.1002/rcs

the target's surface can not be computed directly. Here we propose a method to solve this problem. We can create a set of points $p_1, p_2 \ldots p_n$, where (x_1, y_i, z_i) are the coordinates of point $p_i (i = 1, 2 \ldots n)$ on the target's surface, as shown in Figure 3a. These points can then be used to fit a plane, using the least squares method. We assume that the plane can be defined as the equation: $ax + by - z + d = 0$. According to the least squares method, we minimize the function *L(a, b, d)*:

$$L(a, b, d) = \sum_{i=1}^{n} (ax_i + by_i + d - z_i)^2 \quad (1)$$

We can get the partial derivatives to a, b and d, and set them to zero. Then we get the equations as follows:

$$\begin{cases} (\sum_{i=1}^{n} x_i^2)a + (\sum_{i=1}^{n} x_i y_i)b + (\sum_{i=1}^{n} x_i)d = 0 \\ (\sum_{i=1}^{n} x_i y_i)a + (\sum_{i=1}^{n} y_i^2)b + (\sum_{i=1}^{n} y_i)d = 0 \\ (\sum_{i=1}^{n} x_i)a + (\sum_{i=1}^{n} y_i)b + nd = 0 \end{cases} \quad (2)$$

A

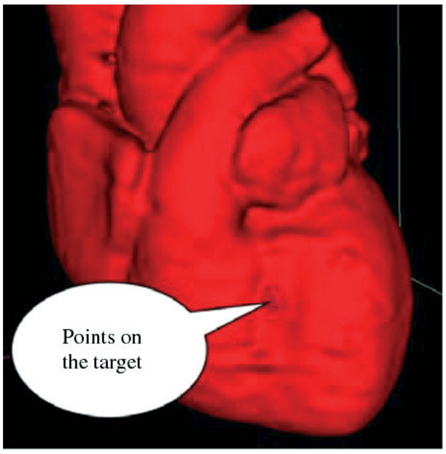

B

Figure 3. Calculation of the target. (a) Points on the target; (b) the target and its normal

We find a, b and c using the equations (2). That is to say, $ax + by - z + d = 0$ is the plane which those points fit. We can consider the normal of the plane as the normal of the target and $(\overline{x}, \overline{y}, \overline{z})$ as the centre of the target ($\overline{x} = \sum_{i=1}^{n} x_i$, $\overline{y} = \sum_{i=1}^{n} y_i$, $\overline{z} = \sum_{i=1}^{n} z_i$) (Figure 3b).

Computing the candidate positions for ports and their normals

Because the ports are placed in the intercostal spaces, the candidate positions should also be put in the space between two adjacent ribs. The edge of a rib could be considered as a curve. Thus, we can calculate a curve between two ribs which fits the surface of the chest wall between the two ribs well, and obtain the candidate positions along the curve. The spline is always used to create a curve according to the control points. The cardinal spline is a cubic spline which provides a compromise method between the flexibility and calculation speed, requiring less computation and storage space. It is more stable than the higher polynomial and is more flexible in simulating arbitrary curve shape than the lower polynomial (17).

A cardinal spline is completely conformed by four control points, so the control points should first be defined. We calculate the middle points between two adjacent ribs as the control points (Figure 4a). After the control points are placed between two ribs, as shown in Figure 4b, a curve can be computed and a series of candidate points can be obtained along the curve with a specific interval, as shown in Figure 4c.

The next step is to compute the normal of each candidate point. The normal of the candidate point should be the same as the normal at the position of the candidate point on the chest wall's surface. We can get a normal plane at any point on the cardinal spline. The normal needed is in the plane. The plane confirmed by the control points can be used to find its normal.

As Figure 5 shows, the green plane is confirmed by three of four red points along the edge of the rib which confirm two control points of a cardinal spline at the spline's two ends. The normal plane grossly expresses the direction of the chest wall's surface at the spline's region. So, we propose a method to get the normal of a candidate point using this plane and its normal plane, i.e. the normal which is perpendicular to the intersection line of those two planes. Figure 6a shows the result of this method.

Selection of ports from candidate points

After creation of the candidate points on the intercostals around the target (Figure 6b), the ports for the thoracoscope and instruments are selected from the candidate points. First, we calculate the α, β angle and the distance of each candidate point to the target. Next, we remove the candidate points whose distances to the target are longer than the length of the instrument, according to the first criterion above. Then the candidate point

DOI: 10.1002/rcs

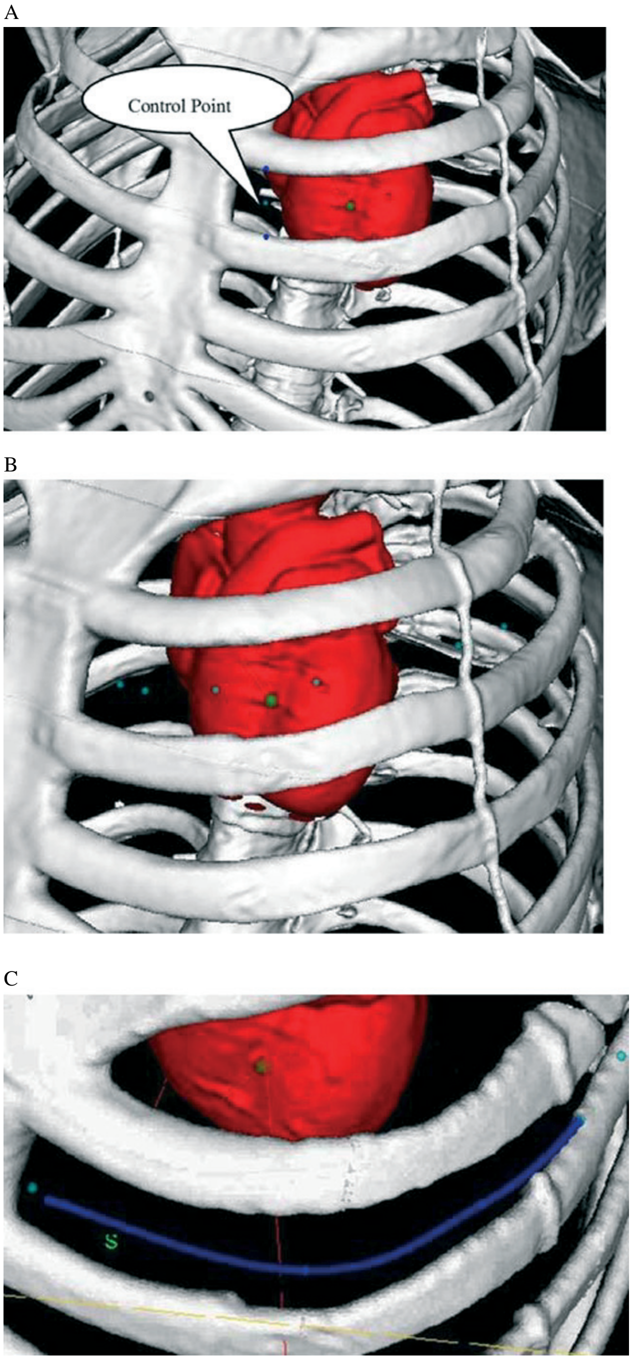

Figure 4. Creation of control points. (a) Creation of one control point; (b) a series of control points between two ribs; (c) a series of candidate points on a cardinal spline between two ribs

which has the smallest α angle is selected as the port for the thoracoscope, according to the second criterion above, and it also is removed from the set of candidate points. The next step is to choose the ports for the surgical instruments. This is more complicated than the selection of the thoracoscope port. We take every combination of two points from the set of candidate points and make them form a triangle with the thoracoscope port. Taking the line segment between the two surgical instrument points as the baseline, its length and the lengths of the other two sides are calculated. An evaluation value is proposed according to criteria 3 and 4 and given to every triangle. The triangle which has the biggest value will be selected and two of its points will be used as the ports for surgical instruments. The evaluation value which considers four factors is expressed as follows:

$$f_1 \times \overline{\beta} + f_2 \times \beta_e + f_3 \times h + f_4 \times s_e \qquad (3)$$

where $\overline{\beta}$ is the average of the β angles of the triangle's two candidate points. In cases of excessive difference between the two β angles, β_e, which is the quotient of the smaller β angle divided by the by longer one, is considered; h is the length of the baseline. According to criterion 4, the lengths of two non-baseline sides should be as equivalent as possible; thus, s_e, which is the quotient of the shorter side divided by the longer side, is considered.

Because $\overline{\beta}$ and the h have different dimensions, we use $\overline{\beta} = \frac{\overline{\beta}}{\overline{\beta}_{\max}}$ and $h = \frac{h}{h_{\max}}$ to solve the problem ($\overline{\beta}_{\max}$ is the largest of all $\overline{\beta}_s$ and $h_{\max}$ is the largest of all hs). β_e and s_e are ratios, so they do not have this problem. f_i ($i = 1$, 2, 3, 4) are the weights of the factors and the sum of them is 1. The user can choose different f_i as needed. Figure 7 shows a result of port placement planning.

Real-time tracking module

In the real-time tracking module, an optical tracker (NDI Polaris, NDI, Waterloo, Canada) is employed. The highly reflective spheres, which can be detected by the tracker, are attached to the surgical instruments and the thoracoscope. The orientation of the instrument and its tip position (for the thoracoscope, this is the position of the centre of the lens) are calculated according to the data transferred from the tracking device.

Registration

Before the real-time tracking process, our system provides the necessary registration for the mapping of virtual space in the PC to the real-world space. Registration depends on some landmark sets in the CT data. The registration is done under a linear transform, in a least squares manner.

Tracking

After registration, a modelled 3D representation of the surgical instruments and thoracoscope are shown correctly in the scene (Figure 8). The orientations of the thoracoscope and surgical instruments and the positions of their tips are obtained. The results serve as input to a real-time alarm module.

Image matching for the target's location

Image matching is the process of detecting a certain anatomical pattern feature from video images (Figure 9)

DOI: 10.1002/rcs

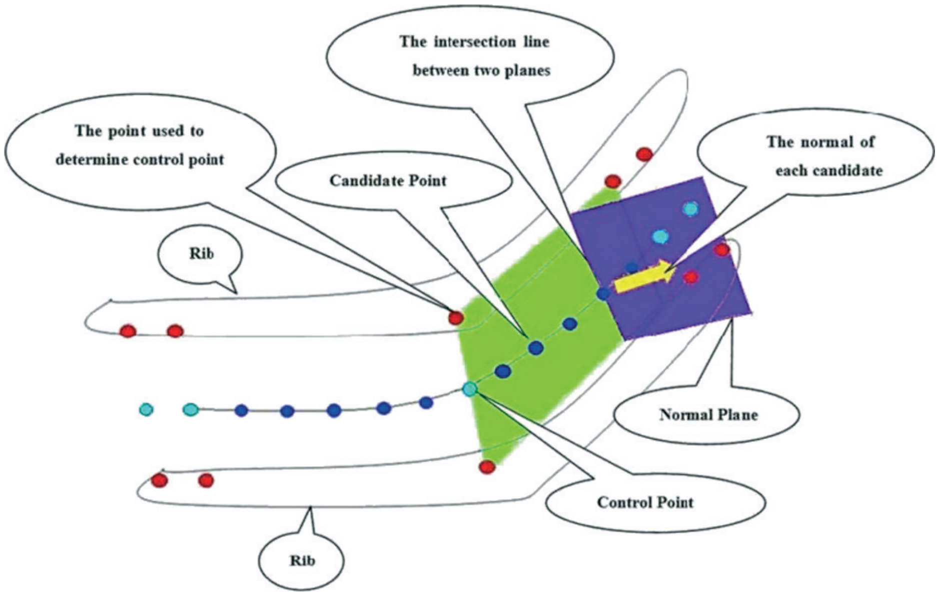

Figure 5. Calculation of the normal of the candidate point

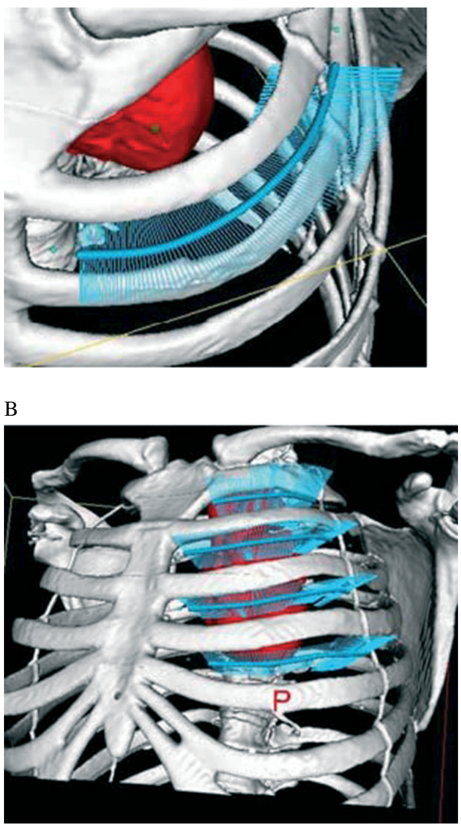

Figure 6. Normals of the candidate points. (a) Candidate points in one intercostal; (b) candidate points on the intercostals around the target

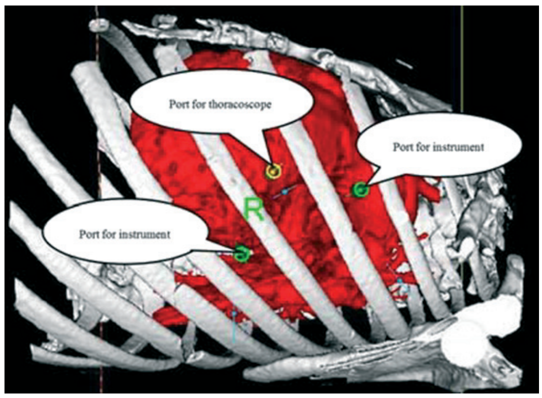

Figure 7. A result of port placement planning

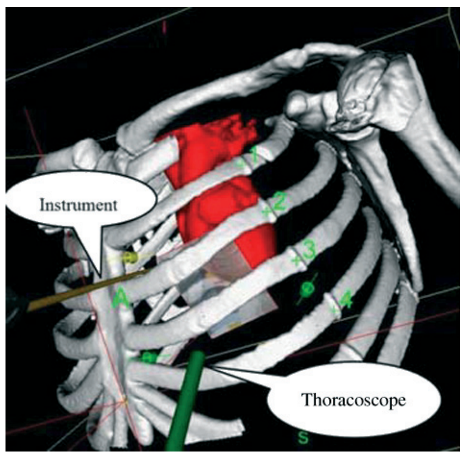

Figure 8. Models of instruments and thoracoscope

in real time. During surgery, image matching to the thoracoscopic video image can help the surgeon locate the target and instruments more accurately. Using a fuzzy matching method (18) based on colour information and greyscale features, the target and the instruments can be located accurately.

Before surgery, we obtain the template image of the target or instrument, and use this image to match the target in the thoracoscopic video during surgery, using the fuzzy matching method.

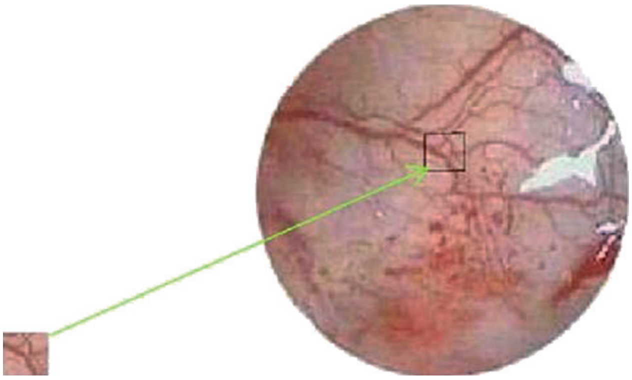

Figure 9. Sub-image and the image where it is matched

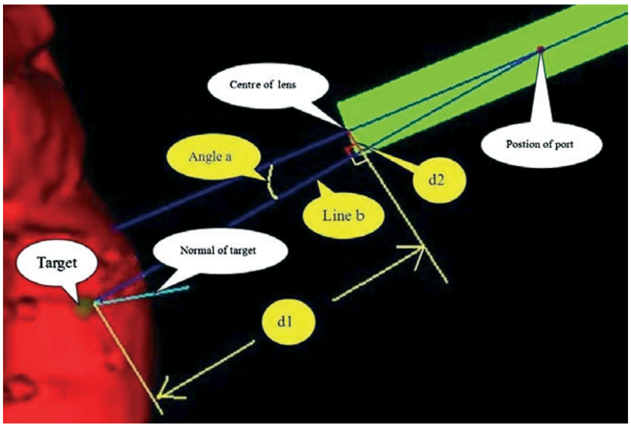

Figure 10. States of the tracked thoracoscope

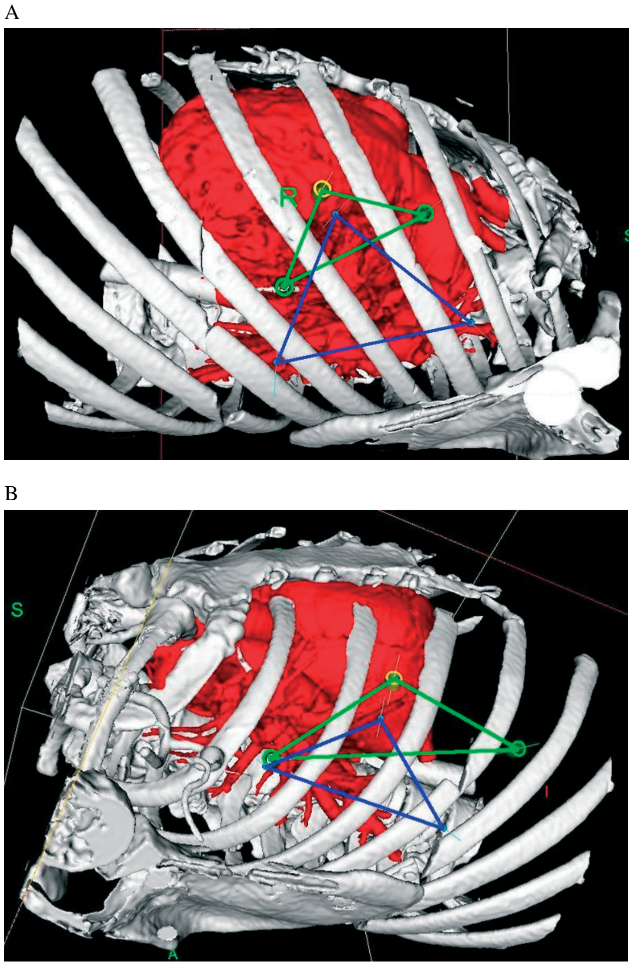

Figure 11. Optimum port placement and experience port placement: (a) CABG; (b)ASR

Alarm module

This module monitors the state of the thoracoscope, so that the surgeon can get a better view while using the thoracoscope. As shown in Figure 10, b is the line connecting the target and the centre of the port; d1 is the distance between the tip of the thoracoscope and the target along the line b, d2 is the distance from the tip centre of the thoracoscope to line b; and a is the angle between the direction of the thoracoscope and the direction of the line b. If the thoracoscope enters the chest along the line b, it will get the best view, where the target will be in the centre of view. Angle a and distance d2 show the degree of departure between the thoracoscope and the line b. The smaller both a and d2 are, the better will be the view obtained. The system monitors the three parameters (d1, d2 and a) of the thoracoscope. When one of the parameters surpasses a specific (threshold) value set before a surgery, the system will register an alarm.

Results

The data of port placement planning

According to the literature, the experience positions of the ports in CABG (19–22) and ASR (23–25) are shown in Table 1. Figure 11a, b shows examples of CABG and ASR, respectively. The green triangles are the optimum positions and the blue triangles are the experience positions.

Case studies for five CABG patients and five ASR patients were performed, using both the traditional port placement method and the proposed planning system. Tables 2 and 3 show the data from the CABG and ASR studies, respectively, where $\overline{x}$ denotes the mean and the s is the standard deviation.

Table 1. Experience positions for CABG and ASR

	CABG	ASR
Endo port	Mid-clavicular line at the fourth intercostal	Mid-clavicular line at the fourth intercostal
Left instrument port	Mid-axillary line at the sixth intercostal	Mid-axillary line at the sixth intercostal
Right instrument port	Mid-axillary line at the third intercostal	Mid-axillary line at the third intercostal

Table 2. Data for CABG

Patient no.	Experience port angle for thoracoscope (°)	Optimum port angle for thoracoscope (°)	Experience port angle for left instrument (°)	Optimum port angle for left instrument (°)	Experience port angle for right instrument (°)	Optimum port angle for right instrument (°)	The value of criterion 4 for experience port	The value of criterion 4 for optimum port
1	65.95	21.927	16.86	59.02	49.01	57.14	0.39	0.41
2	45.76	24.768	57.04	64.15	52.54	62.61	0.40	0.42
3	43.03	26.802	34.91	66.81	51.39	64.72	0.43	0.38
4	59.53	19.07	45.89	58.04	45.652	57.37	0.42	0.40
5	24.30	23.855	49.85	62.69	44.7	60.43	0.41	0.43
$\bar{x} \pm s$	47.71 ± 16.17	23.28 ± 2.93	40.91 ± 15.65	62.14 ± 3.63	48.66 ± 3.44	60.45 ± 3.29	0.410 ± 0.0158	0.408 ± 0.0192

Table 3. Data for ASR

Patient no.	Experience port angle for thoracoscope (°)	Optimum port angle for thoracoscope (°)	Experience port angle for left instrument (°)	Optimum port angle for left instrument (°)	Experience port angle for right instrument (°)	Optimum port angle for right instrument (°)	The value of criterion 4 for experience port	The value of criterion 4 for optimum port
1	52.24	22.52	41.5	45.36	27.83	42.87	0.42	0.37
2	76.1	25.71	38.82	40.23	52.06	46.45	0.40	0.43
3	30.99	20.58	48.97	48.04	44.84	47.83	0.41	0.39
4	42.29	21.24	32.07	49.62	34.67	48.67	0.39	0.40
5	30.41	23.69	49.43	44.47	44.57	43.81	0.44	0.39
$\bar{x} \pm s$	46.40 ± 18.88	22.75 ± 2.04	42.16 ± 7.29	45.54 ± 3.61	40.79 ± 9.53	45.93 ± 2.51	0.412 ± 0.0172	0.396 ± 0.0196

Verifying registration accuracy

The system was run on a normal PC (CPU, Intel® Pentium™ 4, 2.66 GHz; memory size, DDR 2.0 GB; graphics card, nVIDIA® GeForce™, 8500 GT).

We designed an experiment to verify the system's accuracy. The experiment was to use a one-surface-open hollow cube-shaped PVA phantom with a specification of 20 × 20 × 20 cm, as shown in Figure 12a. The phantom was scanned with the spacing of 1.25 mm by a Siemens Somatom Sensation 16 CT scanner with dimensions of 180 × 180 × 55 mm. The CT image of the phantom was constructed as shown in Figure 12b.

In this experiment, we verified the accuracy of registration between the intra-surgery real-world space and the space of the preoperative CT image. The accuracy of the registration was calculated as *FRE*, which was obtained by applying equation (4), where x_i is the coordinate of one of the source points, y_i is the coordinate of one of the target points, R is the rotate matrix, t is the translation vector and the N is the number of source points:

$$FRE = \frac{1}{N}\sum_{i=1}^{N} |Rx_i + t - y_i| \qquad (4)$$

When *FRE* is smaller, the accuracy of registration is higher. However, there are always more or fewer errors introduced by different means. We divided the landmarks into several groups which had three different numbers of landmarks (four, six and eight). Each kind of group was tested five times, and the result is shown in Figure 13, which shows that as the mount of the landmark increases, the accuracy become higher. When we used eight landmarks, the average accuracy was 1.08 ± 0.16 mm.

A

B

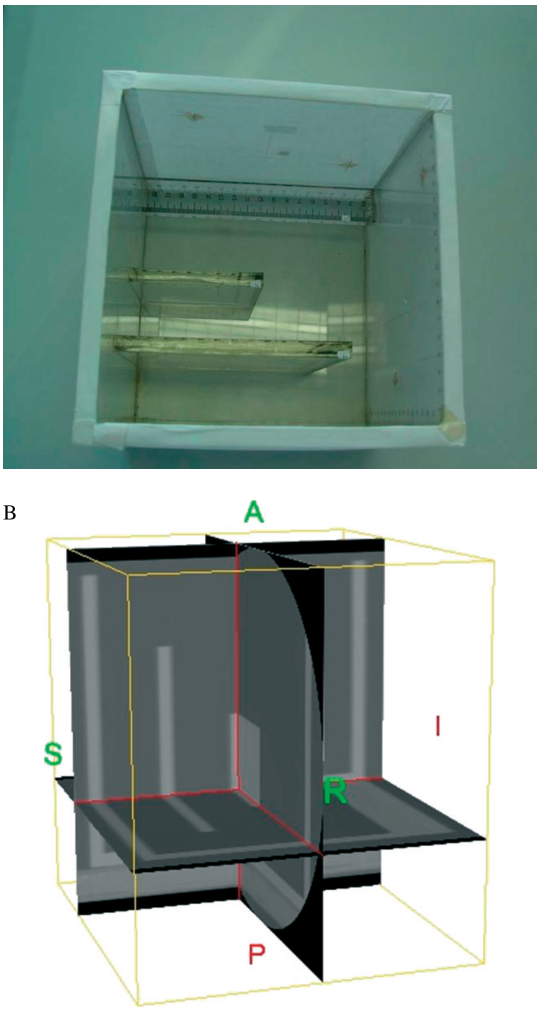

Figure 12. The phantom in this experiment: (a) cube phantom; (b) reconstruction image of phantom

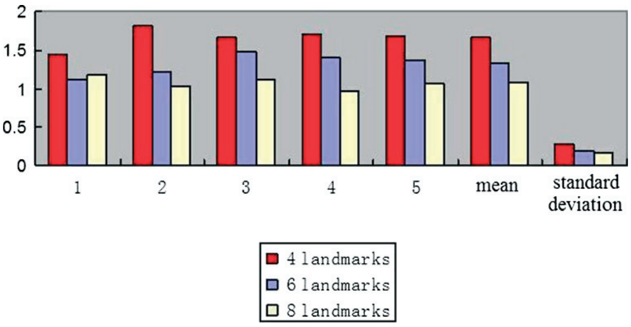

Figure 13. Results of the phantom study

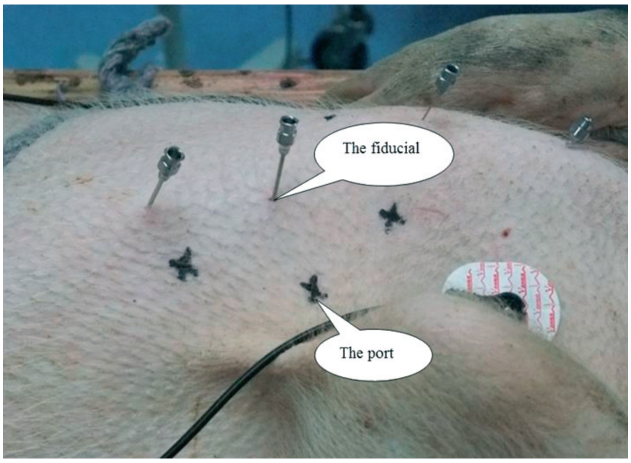

Figure 14. Animal study set-up: the fiducial ports on the pig

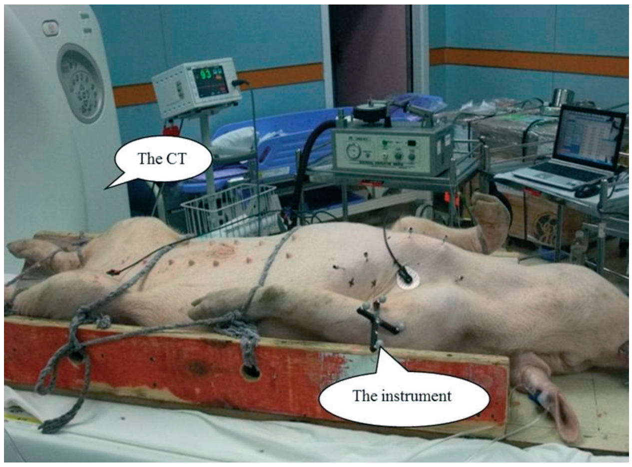

Figure 15. The instrument was fixed to keep its position and was put into the CT machine with the pig

Table 4. Data for animal study

Test no.	Distance from system (mm)	Distance from CT (mm)	Error (mm)
1	8.6	4.1	4.5
2	10.2	15.9	5.7
3	6.6	1.4	5.2
4	11.5	7.3	4.2
5	5.1	11.0	5.9
6	7.6	2.8	4.8

Animal study

Although the anatomical structure of animals differs from that of humans, the criteria of port placement planning would be the same, and can be evaluated using animal testing.

A pig study was involved in our experiment, where six fiducial markers used for registration were pasted on the pig's chest (Figure 14). The pig was anaesthetized and its heart rate was reduced to 70–90 beats/min with drugs during the surgery. The thoracoscope, a Richard Wolf 5507 3CCD Endocam, and the light, a Richard Wolf 5123 Auto LP, and a robot, the Aesop 3000 (Computer Motion) (Figure 15), were employed to control the thoracoscope.

After the port placement planning was automatically performed in the porcine CT image, a landmark-based registration was conducted. Under the guidance of the system, we found the positions of the ports on the pig and made these incisions (Figure 14). Then thoracoscope and the instruments were inserted into the porcine chest, where the thoracoscope and the instruments were monitored under real-time surgical navigation, and the orientation, positions and the relative positions to the target were obtained.

The next step was to test the error of the whole system. With the help of image matching and the navigation system, the approximate region of the target can be located easily, as shown in the Figure 16. We caused the tip of one instrument to arrive at the surface of the porcine heart, near the target position, and obtained the distance between the tip and the target from the system. The instrument was then fixed with the pig to keep its position and was put back into the CT machine (Figure 15) while the real distance was measured using the scanned CT images (Figure 16). The error could be calculated from the two distances, regarding the distance from CT as the golden standard. We obtained the data as shown in Table 4 after the measurements had been repeated six times. The data show that the system error was 5.05 ± 0.67 mm.

Discussion

Specification of the 3D modelling of the surgical instruments and software calculation are the main factors influencing the system error, furthermore the heart beating induces more difficulties for the cardiac navigation system. The accuracy data from the animal studies reflected the complexity, which achieved less accuracy compared to navigation systems for neural and orthopaedic surgery.

The orientation and position of the instruments and of the thoracoscope are calculated according to their position relative to the attached optically-tracked passive spheres. The relative positions of the instruments' tips are gained from a 'pivot' operation, done by manually pivoting the instrument, which will inevitably introduce the error (26).

DOI: 10.1002/rcs

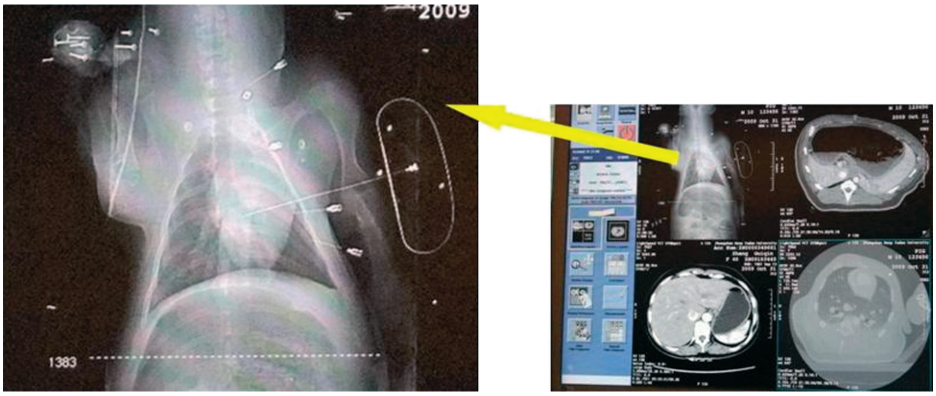

Figure 16. The real distance was measured in the CT image

However, the centre of the thoracoscope lens is not a tiny part and can not be considered as a point in the pivot operation, so the pivot operation is not suitable for the thoracoscope. Shahidi *et al*. (27) proposed a method to solve this problem. We applied their approach in our method to get the offset position in the coordinate system of the reflective ball markers. After all, the accuracy of the system meets the clinical needs so far, based on our experimental evaluation.

The proposed optimization criteria in this paper are independent of the individual anatomy. We used the relative parameters of the optimization criteria, such as the α and β angles, to screen the port positions from the candidate port points, which were based on clinical experience and geodesic measurements from a large number of patients. Although there exists anatomical variability in humans, the screen process can overcome the negative impact. These optimization criteria were also tested by routine surgery planning in our collaborating hospitals.

As shown in Tables 2 and 3, the optimal ports for the thoracoscope in CABG and ASR surgeries had a smaller α angle than those obtained by experience, which results in a much better view, according to criterion 2. The optimal ports for the surgery instruments achieved bigger β angles than ports obtained by the traditional method, so the optimal ports could provide more flexible room, according to criterion 3. Also, the s of optimal ports are smaller than ports obtained by the traditional method, and they are more stable. We conclude that the optimal port placement approach is a significant improvement on traditional port placement planning. The eighth and ninth rows of these tables show the value based on criterion 4, using expression (3) ($f_3 \times h + f_4 \times s_e$). It reveals that the traditional and optimal mothods have good correlation in this aspect, and both values are close to the maximum 0.5. Both the traditional method and the optimal positioning method can provide 'comfortable' operations and have a low possibility of collision between the surgical instruments. However, the optimal ports have a better view and flexibility benefits from the balance of the optimization criteria, which is considered superior to the traditional method.

In the ASR, although the AS can be shown in the CT slice views, it can hardly be seen directly from the view of the thoracoscope. Since the surgical instruments arrive at the AS position through the right atrium, we projected the AS to the right atrium surface virtually in our reconstructed model. The projection position is used as our invasive point. However, this would inevitably produce an error, which can be compensated by reconstructing the model using other real-time imaging techniques, such as trans-oesophageal echocardiography (TEE).

In the animal study, the system error is much bigger than the *FRE*. This depends on the following factors: first, the registration points were fixed to the porcine skin, and the skin may slide slightly; second, the heart is beating, while the heart model in the system is static. However, with the help of endoscopic image matching, the surgeon still can locate the target accurately.

The system is based on the computer graphics and quantitative analysis methods. The port placement planning in the system has been operated in a static heart model so far, so one study for the future works is to take a beating heart model into account. Although the system is still not perfect in accuracy, the study shows that the system can play a guiding role in clinical applications and provides a scientific reference to clinical practice.

Conclusion

This paper introduces a novel system to assist in minimally invasive cardiac surgery. The preoperative planning can help surgeons design a surgical plan better than the traditional method. The real-time intra-surgery guidance can make surgeons aware of the states of the instruments and the thoracoscope and help them to locate the target. The preliminary experiments show that the system is acceptable in terms of both efficiency and accuracy. This system was built on the basis of a very fundamental visualization library, VTK, so we can easily implement the surgeons' immediate requirements into the system.

DOI: 10.1002/rcs

Acknowledgement

This research was partially supported by the National Nature Science Foundation of China (60872103) and the Med-X research fund of Shanghai JiaoTong University (2009).

References

1. Linte CA, Wierzbicki M, Moore J, *et al*. In *Towards subject-specific models of the dynamic heart for image-guided mitral valve surgery*, Ayache N, Ourselin S, Maeder A (eds). MICCAI 2007, Part II, LNCS 4792, 2007; 94–101.
2. Szpala S, Wierzbicki M, Guiraudon G, *et al*. Real-time fusion of endoscopic views with dynamic 3D cardiac images: a phantom study. *IEEE Trans Med Imaging* 2005; **24**(9).
3. Loulmet D, Carpentier A, d'Attellis N, *et al*. Endoscopic coronary artery bypass grafting with the aid of robotic assisted instruments. *J Thorac Cardiovasc Surg* 1999; **118**: 4–10.
4. Chiu AM, Dey D, Drangova M, *et al*. 3D image guided for minimally invasive robotic coronary artery bypass. *Heart Surg Forum* 2000; **3**: 224–231.
5. Sorensen TS, Therkildsen SV, Makowski P, *et al*. A new virtual reality approach for planning of cardiac interventions. *Artif Intell Med* 2001; **22**: 193–214.
6. Austad A, Elle OJ, Rotnes JS. Computer-aided planning of trocar placement and robot settings in robot-assisted surgery. *Int Congress Ser* 2001; **1230**: 1020–1026.
7. Coste-Maniere E, Adhami L, Mourgues F, *et al*. Optimal planning of robotically assisted heart surgery: transfer precision in the operating room. In *Experimental Robotics VIII: Tracts in Advanced Robotics*, Siciliano B, Dario P (eds). Springer: Berlin, 2003; 424–434.
8. Adhmai L, Coste-Maniere E. A versatile system for computer integrated mini-invasive robotic surgery. In *Medical Image Computing and Computer-assisted Intervention* (MICCAI 2002), Dohi T, Kikinis R (eds). Springer: Berlin, 2002; 272–281.
9. Adhmai L, Coste-Maniere E. Optimal planning for minimally invasive surgical robots. *IEEE Trans Robotics Autom* 2003; **19**: (special issue on medical robotics): 854–863.
10. Wierzbicki M, Peters TM. Determining epicardial surface motion using elastic registration: towards virtual reality guidance of minimally invasive cardiac interventions. MICCAI 2003, LNCS 2878, 2003; 722–729.
11. http://www.vision.ee.ethz.ch.
12. http://www-sop.inria.fr/epidaure/epidaure-eng.html.
13. http://www.crd.ge.com/esl/cgsp/projects/medical.
14. Gamma E, Helm R, Johnson R, *et al*. *Design Patterns*. Addison-Wesley: Boston, USA, 1998.
15. Adhami L, Coste-Maniere E, Boissonnat JD. Planning and simulation of robotically assisted minimal invasive surgery. In *Proceedings of Medical Image Computing and Computer-assisted Intervention* (MICCAI 2000). Springer-Verlag: Berlin, 2000; 624–633.
16. Cannon JW, Jeffery AS, Shaun DS, *et al*. Port placement planning in robot-assisted coronary artery bypass. *IEEE Trans Robotics Autom* 2003; **19**(5): 912–917.
17. Hearn D, Baker MP. *Computer Graphics with OpenGL*, 3rd edn. Pearson Education: New Jersey, USA.
18. Tiance H. Research on Surgery Navigation and Visual Location in Robotic-aided Minimally Invasive Cardiac Surgery. Unpublished Master's dissertation, Shanghai Jiaotong University, 2008.
19. Boyd WD, Desai ND, Kiaii B, *et al*. A comparison of robot-assisted versus manually constructed endoscopic coronary anastomosis. *Ann Thorac Surg* 2000; **70**: 839–843.
20. Boatti J, Schachner T, Bonaros N, *et al*. Technical challenges in totally endoscopic robotic coronary artery bypass grafting. *J Thorac Cardiovasc Surg* 2006; **131**: 146–153.
21. Farhat F, Aubert S, Blanc P, *et al*. Totally endoscopic off-pump bilateral internal thoracic artery bypass grafting. *Eur J Cardiothorac Surg* 2004; **26**: 845–847.
22. Mishra YK, Wasir H, Sharma K, *et al*. Totally endoscopic coronary artery bypass Surgery [J]. *Asian Cardiovasc Thorac Ann* 2006; **14**: 447–451.
23. Morgan JA, Peacock JC, Kohmoto T, *et al*. Robotic techniques improve quality of life in patients undergoing septal defect repair. *Ann Thorac Surg* 2004; **77**: 1328–1333.
24. Bonaros N, Schachner T, Oehlinger A, *et al*. Robotically assisted totally endoscopic atrial septal defect repair: insights from operative times, learning curves, and clinical outcome. *Ann Thorac Surg* 2006; **82**: 687–693.
25. Argenziano M, Coz M, Kohmoto T, *et al*. Totally endoscopic atrial septal defect repair with robotic assistance. *Circulation* 2003; **108**(suppl II): 191–194.
26. Northern Digital Inc. *Programming and Application Manual*. Northern Digital: Waterloo, Canada.
27. Shahidi R, Bax MR, *et al*. Implementation, calibration and accuracy testing of an image-enhanced endoscopy system. *IEEE Trans Med Imaging* 2002; **21**(12): 1524–1535.